Investigation of the effects of Sr and Mn doping on corrosion tribocorrosion and cyclic voltammetry performances of TiO$_2$ nanotubes

Muhammet Taha Acar[1*]

[1]Erzincan Binali Yıldırım University, Faculty of Engineering, Department of Mechanical Engineering, Erzincan, Turkey

Abstract: In this study, manganese (Mn) and strontium (Sr) were doped into TiO$_2$ nanotubes (TNT), which are frequently used in energy storage equipment. The aim of this study is to compare the corrosion tribocorrosion and cyclic voltammetry performances of doped TNTs after examining their structural characteristics. XRD and SEM were used to characterize the nanotubes. After the anodization processes, the inclusion of Mn and Sr in the TNT structure was confirmed by XRD analysis. In SEM analysis, it was observed that with the addition of Mn and Sr into the solution, longer nanotubes were formed with increased electrical conductivity. Increasing the nanotube length and shrinking the nanotube's inner diameter provided increased corrosion resistance. Increased surface hardness resulted in increased tribocorrosion resistance. Sr and Mn doping processes increased the corrosion and tribocorrosion resistance compared to undoped TNT, and the highest corrosion and tribocorrosion resitance was obtained from the Sr doped sample. In cyclic voltammetry experiments, the capacitance increased approximately 5 times in Sr-doped TNT compared to undoped TNT, while it increased 10 times in Mn-doped TNT.

Keywords: TiO$_2$ nanotube, Manganese, Strontium, Cyclic voltammetry, Corrosion.

1. Introduction

Today, the production of many technological applications has increased the need for sustainable energy[1]. The need for efficient energy storage equipment to provide sustainable energy has encouraged investments and scientific studies in this field [2]which is the most studied and widely commercialised RFB. The recent expiry of key patents relating to the electrochemistry of this battery has contributed to significant levels of commercialisation in, for example, Austria, China and Thailand, as well as pilot-scale developments in many countries. The potential benefits of increasing battery-based energy storage for electricity grid load levelling and MW-scale wind/solar photovoltaic-based power generation are now being realised at an increasing level. Commercial systems are being applied to distributed systems utilising kW-scale renewable energy flows. Factors limiting the uptake of all-vanadium (and other. Among the efficient energy storage equipment, supercapacitors (SCs) have attracted attention due to their good power densities, high speed performance and long cycle life [3].

But the performance of SCs is affected by many parameters [4]. In practical energy storage applications, the most common problems with SCs are low conductivity, easy dissolution, and low specific capacitance [5]. Therefore, many production methods have been developed in order to produce more efficient SCs by trying to overcome these disadvantages [6-9].

Electrodeposition method, which is one of the SCs production methods, is among the most preferred methods due to its advantages such as rapid preparation, simple use and easy control [10]. When the studies on the production of SCs by the electrodeposition method were examined, it was seen that the use of TiO$_2$ nanotubes (TNT) was preferred in most of them [11, 12]. TNTs are an important semiconductor material with good chemical stability, low cost, low toxicity and environmentally friendly nature[13]. In addition, being easy to produce and synthesizing in the desired size provides a great advantage in the production of SCs [14]. However, when TNTs are used alone as electrode material, their capacitance is relatively low [15]. For this reason, many scientific studies have been carried out to increase the capacitance of TNT [16-19].

It has been seen that manganese (Mn) and strontium (Sr) are used in most of the studies on increasing the TiO$_2$ capacitance. Ning et al. [20] prepared Mn-doped TiO$_2$ micro/nano structured porous film by anodizing Ti-Mn alloy containing 10.0% Mn by weight, and they emphasized that superior field capacitance and excellent capacitive properties such as 1451.3 mF/cm^2 were obtained. Shahabuddin et al. [21] in their study using SrTiO$_3$, they also stated that they achieved an excellent stability cycle

* Corresponding author.
Email: taha.acar@erzincan.edu.tr

with 114% capacity retention after 4000 cycles. Zhang et al. [22] emphasized that the MnO_2 electrode exhibited the best electrochemical performance with its high specific capacitance.

In this study, Mn-doped TNT and Sr-doped TNTs were synthesized by electrodeposition method on TNTs, which are preferred to be used in SCs production. The aim of this study is to compare the corrosion tribocorrosion and cyclic voltammetry performances of TNTs after examining their structural characteristics. X-ray diffractometer (XRD) and scanning electron microscope (SEM) were used for the structural characterization of the anodic films. In addition, their electrochemical properties were studied using potentiodynamic polarization and cyclic voltammetry (CV).

2. Experimental details

In this study, Cp-Ti samples whose chemical composition was given in the previous study were used [23]. TNT synthesis was carried out by applying all procedures as described in the previous study with 150 V and 2 h parameters applied in the anodizing process [19]. The positive electrode was Cp-Ti samples and the negative electrode was a graphite rod. The separation between them was predetermined to be 30 mm during anodizing. All samples underwent anodizing using a direct current (DC) power source. Sample groups used in this study are given below:

- Untreated Cp-Ti

- TNT synthesized on Cp-Ti = TNT

- Manganese doped TNT= Mn-doped TNT(in aqueous solution containing 10.0 wt% Mn)

- Strontium doped TNT= Sr-doped TNT (in aqueous solution containing 10.0 wt% Sr)

A XRD-GNR-Explorer X-Ray diffraction equipment was used with a Cu-Kα (λ=1.54059 Å) source at 40 kV and 30 mA to identify the phase of Cp-Ti samples using a 2θ scale between 10° and 90°. By comparing them to the International Diffraction Data Center (ICDD) standard cards, all phases were identified. Using the FEI QUANTA 250 Scanning Electron Microscope, top and cross-section images were captured.

Electrochemical experiments were performed using Potentiodynamic Polarization and Cyclic Voltammetry (CV) with GAMRY series G750TM (Gamry Instruments, Warminster, USA) in SBF solution. At human body temperature (37 ± 0,5 ∘C), the corrosion resistance of Cp-Ti samples was examined. The three-electrode technique was used for the electrochemical experiments. Ag/AgCl was used as the reference electrode and graphite as the counter electrode. Chemical composition of SBF and initial parameters in electrochemical experiments were given in the previous study [23].

Tribocorrosion tests were carried out using the Turkyus PODWT&RWT reciprocating tribotester in conjunction with an electrochemical monitoring equipment at 22 °C and 50% relative humidity. After potential equilibration, rubbing tests for tribocorrosion were performed in open-circuit potential settings. Alumina ball with a diameter of 6 mm was used as the pin, and a normal force of 1 N was applied. The reciprocation frequency was 1 Hz, and the stroke length was 8 mm. A 3D surface profilometer was used to investigate the wear track's shape and the anodic films' surface roughness (Bruker Contour GT-K1).

3. Results and discussion

3.1. Structural characterization

The XRD graphs of the TNT, Mn-doped TNT, and Sr-doped TNT are presented in Fig. 1. According to XRD graphics, anatase TiO_2 formation was observed in the base material consisting of alpha titanium structure after TNT synthesis. XRD plot of synthesized Mn-doped TNT shows the diffraction peaks of both MnO_2 and anatase TiO_2. In addition, the anatase TiO_2 diffraction peak of Mn-doped TNT was consistent with pure TNT anatase TiO_2; this indicates that the phase structure of TiO_2 is stable and remains unchanged during the doping process[20]. Also, after doping Sr to TNTs, it is seen in XRD graphs that TiO_2 transforms into strontium titanate [24].
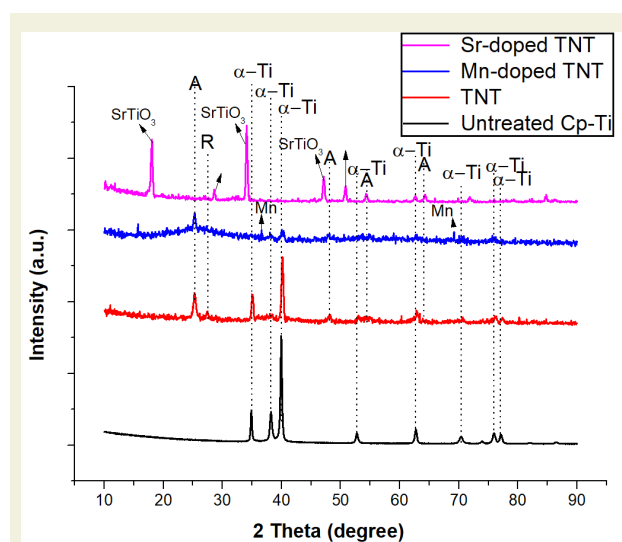

Figure 1. XRD pattern of all samples.

As shown in Fig. 2, uniform undoped nanotubes of about 200 nm in outer diameter and about 9.8 μm in length were produced by anodizing. After doping, the original nanotube array architecture was preserved as seen in SEM images in Fig. 2. However, after doping, the inner diameter of the nanotubes was slightly reduced due to volume expansion during the transformation from titanium oxide to strontium titanate ($SrTiO_3$), and MnO_2 [21]. As can be seen from the cross-section SEM pictures,

the electrical conductivity changed with the introduction of Mn and Sr into the anodization solution, and the changing electrical conductivity affected the length of the nanotubes. The addition of Sr into the solution accelerated the formation of TNT, and the longest nanotubes were obtained from the Sr-doped TNT, which is known to have better electrical conductivity [25].

3.2. Corrosion analyses

Fig. 3 shows the curves for corrosion potential (Ecorr) and corrosion current density (Icorr). The presence of anatase TiO_2 formed on TNT, and the TNT architecture provided increased corrosion resistance compared to untreated material. The inner diameter of TNTs decreased, and the length of the TNTs increased after the doping processes, which can also be seen from the SEM images, and this prevented the SBF from reaching the substrate material, causing a positive shift in the Ecorr values.

Bode and Nyquist plots of all samples are shown in Fig. 4 and simulated EIS results are listed in Table 1. The solution resistance, charge transfer resistance, and constant phase element, respectively, are symbolized by Rs, Rct, and CPE in the equivalent circuit model that is being presented. Rct values representing the charge transfer resistance between the substrate material and the coated film increased after TNT synthesis [26]. The increase in electrical conductivity of Mn and Sr and thus obtaining longer nanotubes provided higher Rct values compared to undoped TNT. Finally, the highest Rct value was obtained in Sr-doped TNT, where the longest nanotubes were obtained.

3.3. Tribocorrosion analyses

The open circuit potential (OCP) graphs obtained during the tribocorrosion tests are given in Fig. 5. When the OCP graphs were examined, it was seen that the lowest average OCP values were obtained from untreated Cp-Ti.
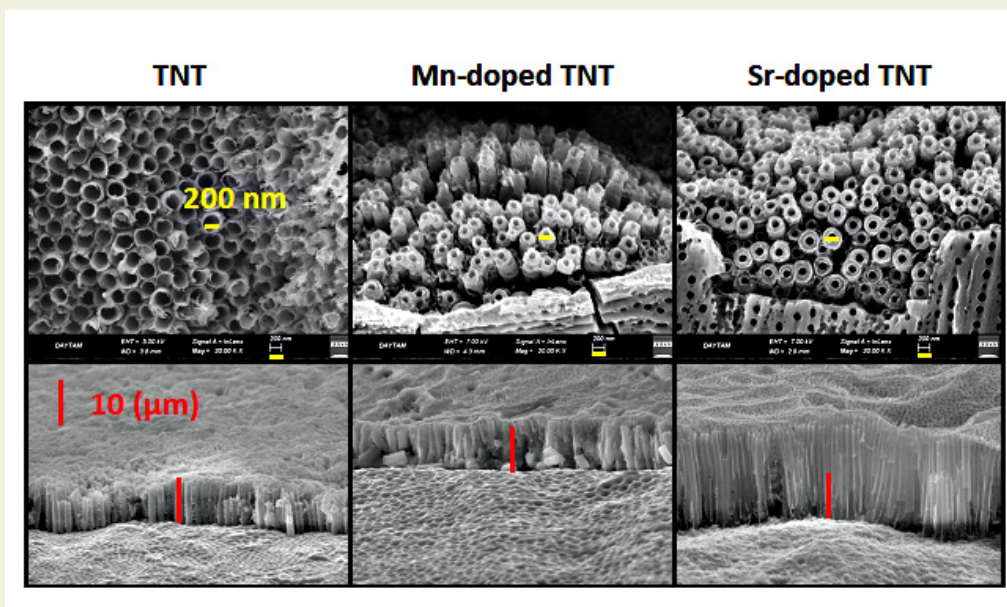

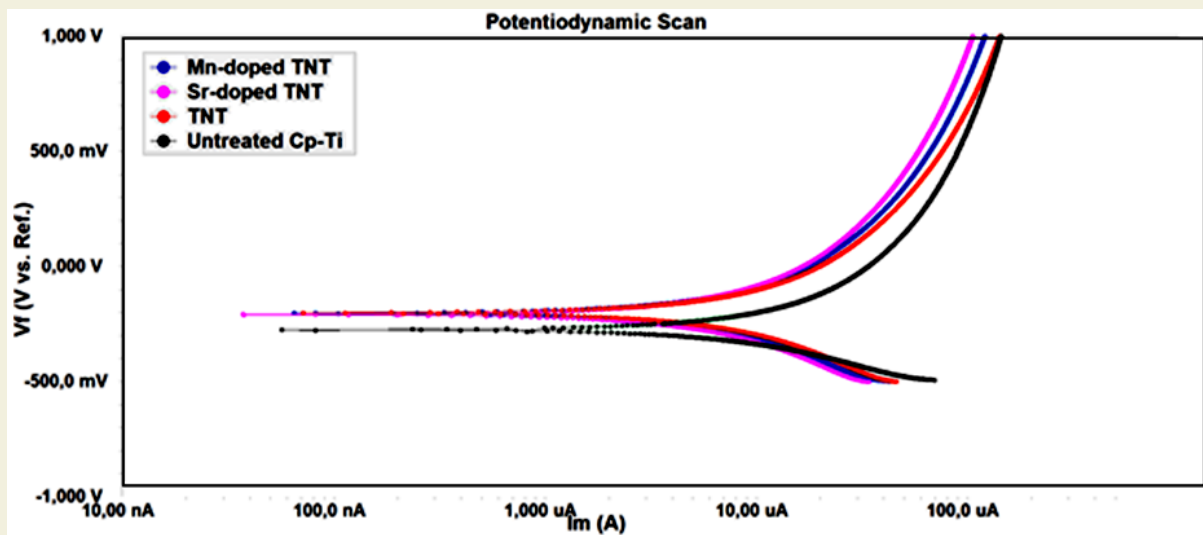**Figure 2.** Top and cross-sectional SEM images of TNT, Mn-doped TNT and Sr- doped TNT.

Figure 3. Potentiodynamic polarization curves of untreated Cp-Ti, TNT, Mn-doped TNT and Sr- doped TNT.
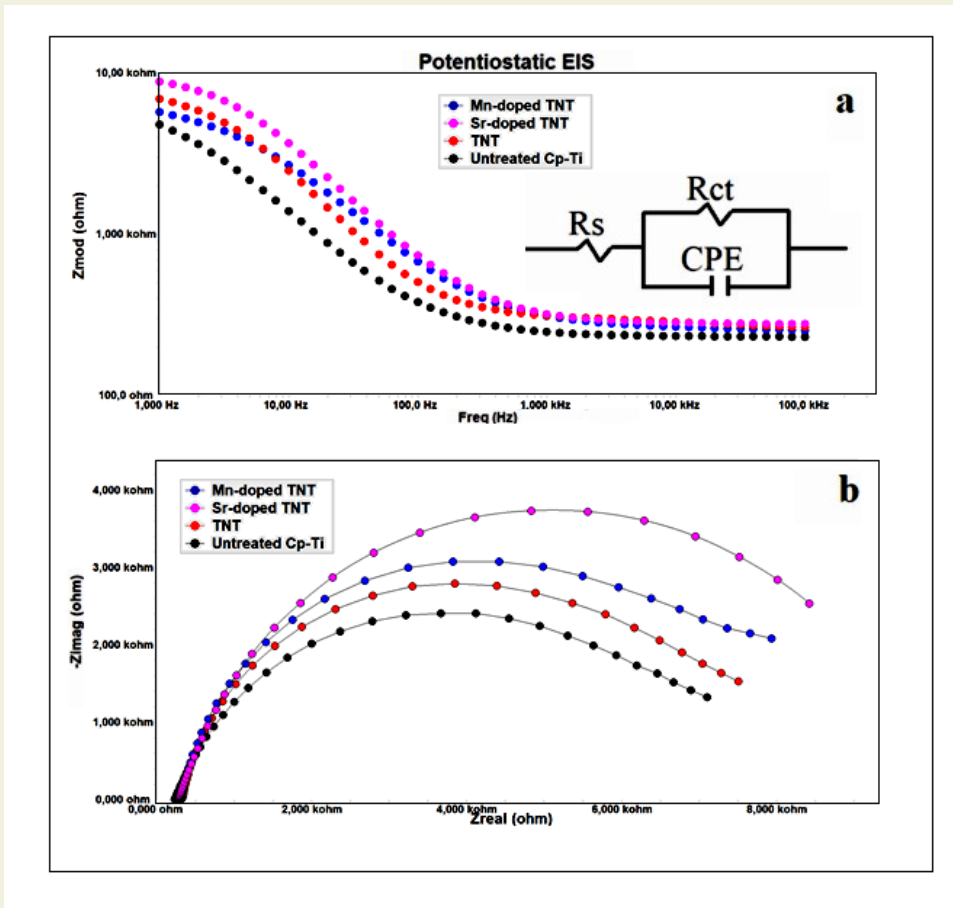
Figure 4. Bode (a) and Nyquist (b) plots of untreated Cp-Ti, TNT, Mn-doped TNT and Sr- doped TNT.
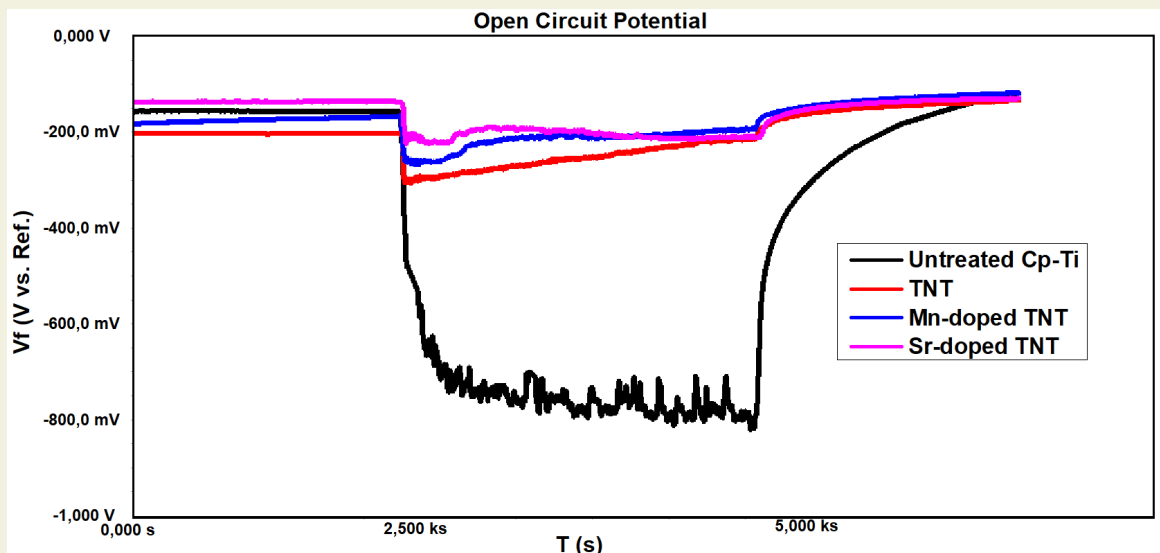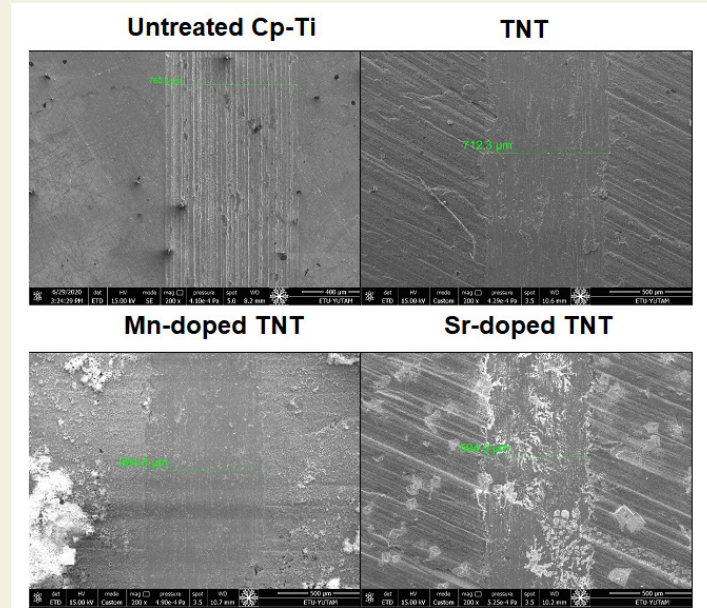

Figure 5. OCP curves of untreated Cp-Ti, TNT, Mn-doped TNT and Sr- doped TNT.

While in the other samples, OCP values showed a nearly linear progression from the beginning to the end of the sliding process, it was observed that there were small increases and decreases during the sliding process in the untreated CP-Ti sample. It can be said that these values obtained from the untreated Cp-Ti sample are due to the fact that the natural oxide layer is more easily separated from the surface during wear and the particles detached from the Cp-Ti surface cause vibration during wear [27]. The untreated Cp-Ti sample had the lowest average OCP values due to the thin natural oxide film [28]. TNTs synthesized on Cp-Ti caused a positive shift of OCP values. The TNT architecture obtained on Cp-ti made it difficult for SBF to reach the base material, causing a positive shift in OCP values. It was observed that the mean OCP values of Undoped, Mn-doped and Sr-doped TNTs were close

Figure 6. Wear trace of untreated Cp-Ti, TNT, Mn-doped TNT and Sr- doped TNT.

Table 1. The corrosion and cyclic voltammetry test results of all sample.

Parameters	E_{corr} (mV)	i_{corr} (A/cm^2)	R_s (Ωcm^2)	R_{ct} (Ωcm^2)	Film thickness (μm)	CV Capacitance 100 mV/s- (mF/cm^2)	Surface roughness (μm)	Hardness (HV$_{0.1}$)	Wear rate (x10^{-3} mm^3/Nm)
Sr-doped TNT	-144	3.83×10^{-6}	74.2	7.6	19.6	15.4×10^{-6}	3.5	720	0.49
Mn-doped TNT	-155	4.18×10^{-6}	70.7	7.1	12.2	29.9×10^{-6}	3.6	650	0.57
TNT	-177	21.9×10^{-6}	66.8	6.3	9.8	2.92×10^{-6}	3.4	570	0.66
Untreated Cp-Ti	-460	103.4×10^{-6}	43.4	2.3	-	-	0.32	350	0.74

to each other. When the wear trace SEM images Fig.7 and Table 1 were examined together, it was seen that the most wear was seen in the untreated Cp-Ti sample, while the least wear was obtained from the Mn doped TNT. After TNT synthesis, increasing surface hardness with anatase TiO2 formed on the surface provided an increase in wear resistance. The highest wear resistance was obtained from the Mn-doped TNT sample, where the highest surface hardness was obtained.

3.4. Cyclic voltammetry analyses
Fig. 8 a-c shows cyclic voltammetry (CV) curves for TNT, Mn-doped TNT, and Sr-doped TNT at scanning rates between 5 and 100 mV/s. Fig. 8 shows the comparison of cyclic voltammetry (CV) curves of TNT, Mn-doped TNT, and Sr-doped TNT samples at a scanning rate of 100 mV/s. After the Mn and Sr doping processes, the specific capacitance increased as seen in Fig.8. This increase in capacitance compared to the undoped TNT sample can be attributed to the increase in nanotube length [29].

When the areas under the CV curves are examined, it is seen that most area is obtained from Mn-doped TNT. The areal capacitance difference between Sr-doped and Mn-doped is attributed to the resistance formed between

the substrate and the nanotubes. In the previous study, it was emphasized that the contact area between the oxide layer and the metal substrate and the electrical conductivity affect the charge transfer resistance, and this is effective in determining the areal capacitance [30]. In summary, the obtain less charge transfer resistance between Mn-doped TNT and the base material resulted in higher areal capacitance.

4. Conclusions

In this study, after examining the structural properties of undoped TNT, Mn-doped TNT and Sr-doped TNT synthesized on Cp-Ti samples, corrosion and cyclic voltammetry performances were compared. According to the experimental data results obtained:

In XRD analysis, it was determined that Mn and Sr added to the anodization solution were included in the TNT structure. When the SEM images were examined, it was seen that the inclusion of Mn and Sr in the TNT structure caused volume expansion and it was determined that the inner diameters of TNTs narrowed compared to undoped TNT. However, the addition of Mn and Sr to the anodization solution increased the electrical conductiv-
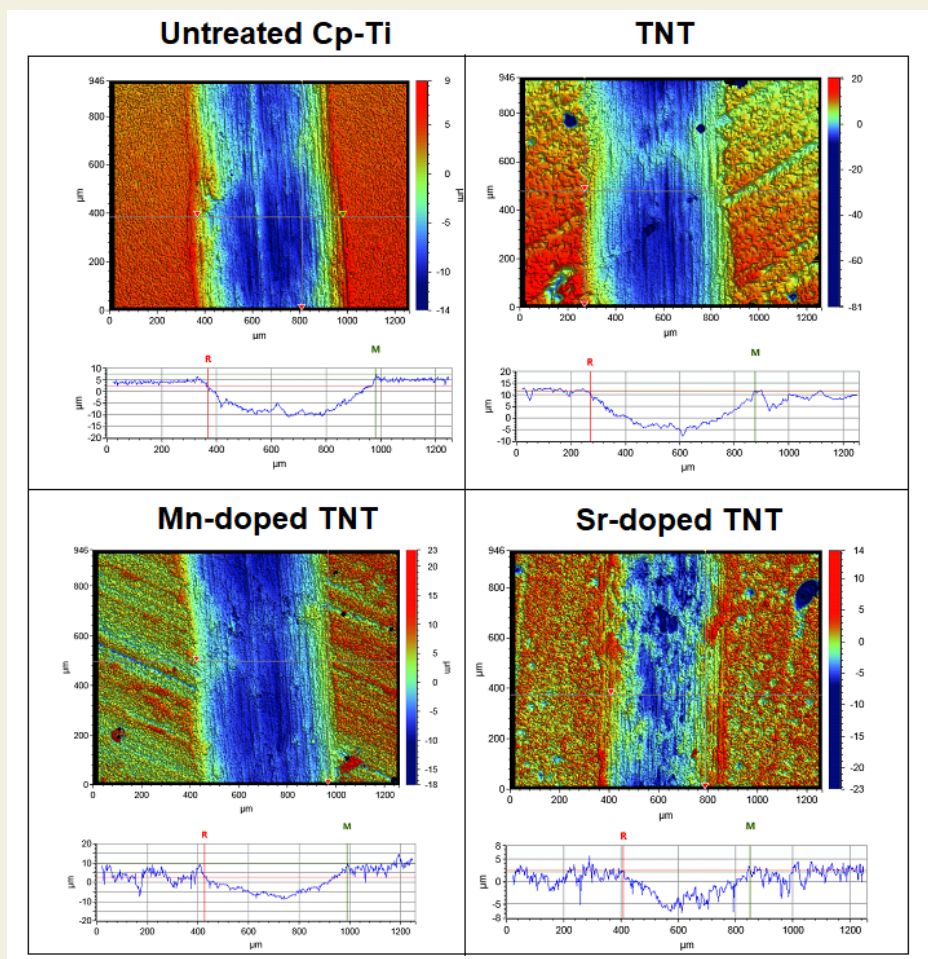
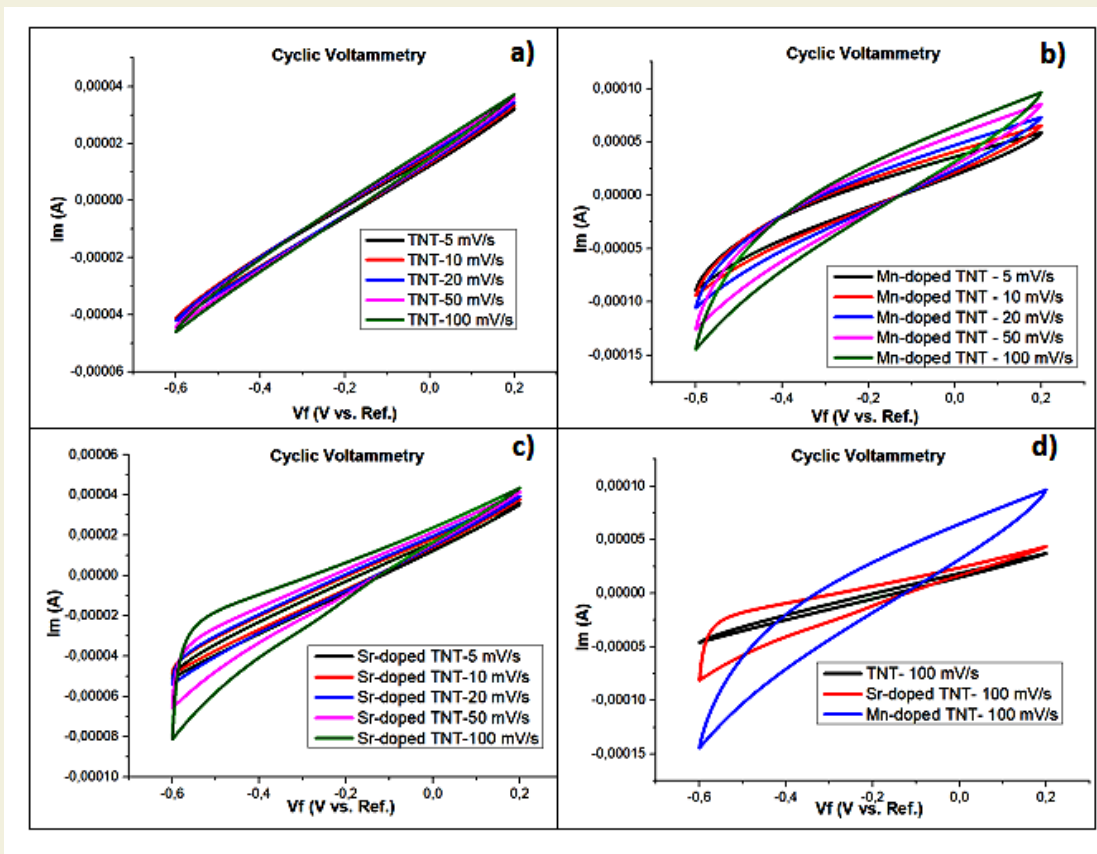**Figure 7.** 3D profilometer images of untreated Cp-Ti, TNT, Mn-doped TNT and Sr- doped TNT.

Figure 8. Cyclic voltammetry curves of TNT, Mn-doped, and Sr-doped TNT.

ity and resulted in the formation of longer nanotubes. It has been observed that the formation of longer lengths and narrower inner diameters of nanotubes as a result of Mn and Sr doping processes to TNT provides an increase in corrosion resistance. Although the OCP values of all TNTs showed similar behaviour in the tribocorrosion test results, surface hardness was the determining parameter in the wear rates. Mn-doped TNT with the highest surface hardness exhibited the best tribocorrosion behaviour. In cyclic voltammetry experiments, while the capacitance increased approximately 5 times in Sr-doped

TNT compared to Undoped TNT, it increased 10 times in Mn-doped TNT. Mn-doped TNT greater capacitance increase was achieved by the formation of lower resistivity between the substrate and the coated film.

5. Declaration of Interest Statement

The authors declare that they have no known competing financial interests or personal relationships that could have appeared to influence the work reported in this paper.

References

[1] H. Chen, R. Yada, Nanotechnologies in agriculture: New tools for sustainable development, Trends Food Sci. Technol. 22 (2011) 585–594. https://doi.org/10.1016/j.tifs.2011.09.004.

[2] G. Kear, A.A. Shah, F.C. Walsh, Development of the all-vanadium redox flow battery for energy storage: a review of technological, financial and policy aspects: All-vanadium redox flow battery for energy storage, Int. J. Energy Res. 36 (2012) 1105–1120. https://doi.org/10.1002/er.1863.

[3] A. Burke, Ultracapacitors: why, how, and where is the technology, J. Power Sources. 91 (2000) 37–50.

[4] S. Zhang, N. Pan, Supercapacitors Performance Evaluation, Adv. Energy Mater. 5 (2015) 1401401. https://doi.org/10.1002/aenm.201401401.

[5] W. Raza, F. Ali, N. Raza, Y. Luo, K.-H. Kim, J. Yang, S. Kumar, A. Mehmood, E.E. Kwon, Recent advancements in supercapacitor technology, Nano Energy. 52 (2018) 441–473.

[6] S. Kour, S. Tanwar, A.L. Sharma, A review on challenges to remedies of MnO2 based transition-metal oxide, hydroxide, and layered double hydroxide composites for supercapacitor applications, Mater. Today Commun. (2022) 104033.

[7] I.T. Bello, A.O. Oladipo, O. Adedokun, S.M. Dhlamini, Recent advances on the preparation and electrochemical analysis of MoS2-based materials for supercapacitor applications: A mini-review, Mater. Today Commun. 25 (2020) 101664.

[8] E.E. Miller, Y. Hua, F.H. Tezel, Materials for energy storage: Review of electrode materials and methods of increasing capacitance for supercapacitors, J. Energy Storage. 20 (2018) 30–40. https://doi.org/10.1016/j.est.2018.08.009.

[9] U. Samukaite-Bubniene, A. Valiūnienė, V. Bucinskas, P. Genys, V. Ratautaite, A. Ramanaviciene, E. Aksun, A. Tereshchenko, B. Zeybek, A. Ramanavicius, Towards supercapacitors: Cyclic voltammetry and fast Fourier transform electrochemical impedance spectroscopy based evaluation of polypyrrole electrochemically deposited on the pencil graphite electrode, Colloids Surf. Physicochem. Eng. Asp. 610 (2021) 125750. https://doi.org/10.1016/j.colsurfa.2020.125750.

[10] R.S. Kate, S.A. Khalate, R.J. Deokate, Overview of nanostructured metal oxides and pure nickel oxide (NiO) electrodes for supercapacitors: A review, J. Alloys Compd. 734 (2018) 89–111.

[11] R. Naraprawatphong, C. Chokradjaroen, S. Thiangtham, L. Yang, N. Saito, Nanoscale advanced carbons as an anode for lithium-ion battery, Mater. Today Adv. 16 (2022) 100290.

[12] Z. Hai, M.K. Akbari, Z. Wei, C. Xue, H. Xu, J. Hu, L. Hyde, S. Zhuiykov, TiO2 nanoparticles-functionalized two-dimensional WO3 for high-performance supercapacitors developed by facile two-step ALD process, Mater. Today Commun. 12 (2017) 55–62.

[13] Y. Zhao, N. Hoivik, K. Wang, Recent advance on engineering titanium dioxide nanotubes for photochemical and photoelectrochemical water splitting, Nano Energy. 30 (2016) 728–744.

[14] S. Specchia, C. Galletti, V. Specchia, Solution combustion synthesis as intriguing technique to quickly produce performing catalysts for specific applications, in: Stud. Surf. Sci. Catal., Elsevier, 2010: pp. 59–67.

[15] S. Yadav, A. Nair, K. Urs MB, V.B. Kamble, Protonic titanate nanotube–reduced graphene oxide composites for hydrogen sensing, ACS Appl. Nano Mater. 3 (2020) 10082–10093.

[16] E. Budak, S. Aykut, M.E. Paşaoğlu, C. Ünlü, Microwave assisted synthesis of boron and nitrogen rich graphitic quantum dots to enhance fluorescence of photosynthetic pigments, Mater. Today Commun. 24 (2020) 100975.

[17] P.R. Deshmukh, S.V. Patil, R.N. Bulakhe, S.D. Sartale, C.D. Lokhande, SILAR deposited porous polyaniline-titanium oxide composite thin film for supercapacitor application, Mater. Today Commun. 8 (2016) 205–213.

[18] M. Paredes-Ramos, F. Bates, I. Rodríguez-González, J.M. López-Vilariño, Computational approximations of molecularly imprinted polymers with sulphur based monomers for biological purposes, Mater. Today Commun. 20 (2019) 100526.

[19] M.T. Acar, H. Kovacı, A. Çelik, Comparison of the structural properties, surface wettability and corrosion resistance of TiO2 nanotubes fabricated on Cp-Ti, Ti6Al4V and Ti45Nb, Mater. Today Commun. 33 (2022) 104396.

[20] X. Ning, X. Wang, X. Yu, J. Zhao, M. Wang, H. Li, Y. Yang, Outstanding supercapacitive properties of Mn-doped TiO2 micro/nanostructure porous film prepared by anodization method, Sci. Rep. 6 (2016) 1–8.

[21] S. Shahabuddin, A. Numan, M.M. Shahid, R. Khanam, R. Saidur, A.K. Pandey, S. Ramesh, Polyaniline-SrTiO3 nanocube based binary nanocomposite as highly stable electrode material for high performance supercapaterry, Ceram. Int. 45 (2019) 11428–11437.

[22] Y. Zhang, Q. Yao, H. Gao, L. Zhang, L. Wang, A. Zhang, Y. Song, L. Wang, Synthesis and electrochemical performance of MnO2/BC composite as active materials for supercapacitors, J. Anal. Appl. Pyrolysis. 111 (2015) 233–237.

[23] M.T. Acar, H. Kovacı, A. Çelik, Improving the wettability and corrosion behavior of Cp-Ti by applying anodization surface treatment with the addition of boric acid, graphene oxide and hydroxyapatite, Mater. Today Commun. (2022) 103683.

[24] Y. Xin, J. Jiang, K. Huo, T. Hu, P.K. Chu, Bioactive SrTiO3 nanotube arrays: strontium delivery platform on Ti-based osteoporotic bone implants, ACS Nano. 3 (2009) 3228–3234.

[25] F. Han, V.S.R. Kambala, M. Srinivasan, D. Rajarathnam, R. Naidu,

Tailored titanium dioxide photocatalysts for the degradation of organic dyes in wastewater treatment: a review, Appl. Catal. Gen. 359 (2009) 25–40.

[26] L. Sun, J. Cai, Q. Wu, P. Huang, Y. Su, C. Lin, N-doped TiO2 nanotube array photoelectrode for visible-light-induced photoelectrochemical and photoelectrocatalytic activities, Electrochimica Acta. 108 (2013) 525–531.

[27] H. Sharifi, M. Aliofkhazraei, G.B. Darband, A.S. Rouhaghdam, Tribological properties of PEO nanocomposite coatings on titanium formed in electrolyte containing ketoconazole, Tribol. Int. 102 (2016) 463–471. https://doi.org/10.1016/j.triboint.2016.06.013.

[28] M. Palacio, B. Bhushan, A Review of Ionic Liquids for Green Molecular Lubrication in Nanotechnology, Tribol. Lett. 40 (2010) 247–268. https://doi.org/10.1007/s11249-010-9671-8.

[29] A. Bandyopadhyay, A. Shivaram, I. Mitra, S. Bose, Electrically polarized TiO2 nanotubes on Ti implants to enhance early-stage osseointegration, Acta Biomater. 96 (2019) 686–693. https://doi.org/10.1016/j.actbio.2019.07.028.

[30] X. Ning, X. Wang, X. Yu, J. Zhao, M. Wang, H. Li, Y. Yang, Outstanding supercapacitive properties of Mn-doped TiO2 micro/nanostructure porous film prepared by anodization method, Sci. Rep. 6 (2016) 22634. https://doi.org/10.1038/srep22634.